Alteration of Water Exchange Rates Following Focused Ultrasound-Mediated BBB Opening in the Dorsal Striatum of Non-Human Primates: A Diffusion-Prepared pCASL Study

Dong Liu[a,b*], Xingfeng Shao[c], Fabian Munoz Silva[a,b], Soroosh Sanatkhani[a,b], Ray Lee[d], Elisa E Konofagou [e,f], Danny JJ Wang [c], Vincent P Ferrera [a,b,g]

[a] Dept. of Neuroscience, Columbia University, New York, NY, USA

[b] Zuckerman Mind Brain Behavior Institute, Columbia University, New York, NY, USA

[c] Stevens Neuroimaging and Informatics Institute, Keck School of Medicine, University of Southern California, Los Angeles, CA, USA

[d] Dept. of Radiology, University of Texas Health Science Center at San Antonio, San Antonio, TX, USA

[e] Dept. of Biomedical Engineering, Columbia University, New York, NY, USA

[f] Dept. of Radiology, Columbia University, New York, NY, USA

[g] Dept. of Psychiatry, Columbia University, New York, NY, USA

*dl3341@columbia.edu

Abstract

This study applied diffusion-prepared pseudo-continuous arterial spin labeling (DP-pCASL) to quantify cerebral blood flow (CBF), arterial transit time (ATT), and blood-brain barrier (BBB) water exchange rate (K_w) before and after focused ultrasound (FUS)-mediated blood-brain barrier opening (BBBO) in the dorsal striatum of four non-human primates. Six baseline and seven BBBO sessions were performed. DP-pCASL was acquired approximately 45 minutes after FUS sonication combined with intravenous microbubbles, and contrast-enhanced T1-weighted imaging was subsequently used to confirm the BBBO region. Whole-brain analyses revealed no significant changes in CBF or ATT following BBBO (permutation $p > 0.05$). Region-of-interest analysis within the sonicated caudate demonstrated a significant localized decrease in K_w, with median (IQR) values of 45.0 (40.6 - 55.6) min^{-1} at the BBBO site versus 61.6 (58.3 - 70.4) min^{-1} in the contralateral control region ($p < 0.05$), confirming spatially specific suppression of transendothelial water flux. In contrast, whole-brain K_w increased significantly following BBBO, with median (IQR) values of 49.8 (46.3 - 55.9) min^{-1} in non-BBBO sessions versus 59.4 (56.6 - 66.3) min^{-1} in BBBO sessions ($p < 0.01$), indicating a diffuse enhancement of water exchange across the brain. These findings establish DP-pCASL-derived K_w as a sensitive, non-contrast biomarker for both local and global BBB permeability changes induced by focused ultrasound, supporting its potential for longitudinal monitoring in preclinical and clinical neurotherapeutic applications.

Keywords:

Diffusion-prepared pseudo-continuous arterial spin labeling (DP-pCASL), focused ultrasound (FUS), blood-brain barrier opening (BBBO), water exchange rates, contrast-free biomarker

Introduction

Focused ultrasound (FUS) combined with intravenously administered microbubbles enables a safe, transient, and localized opening of the blood-brain barrier (BBB) (Aryal et al., 2014; Hynynen et al., 2001; McDannold et al., 2007). This effect is achieved by applying focused acoustic energy that causes circulating microbubbles within targeted cerebral vessels to oscillate (Marquet et al., 2014; Tung et al., 2011), generating mechanical forces that temporarily disrupt endothelial tight junctions (Konofagou, 2012; Sheikov et al., 2004). By temporarily disrupting the BBB, FUS facilitates the delivery of therapeutic agents such as chemotherapeutic drugs, antibodies, and viral vectors into selected brain regions, offering promising treatments for neurological and psychiatric disorders including Alzheimer's disease, Parkinson's disease, and brain cancers (Leinenga et al., 2016; Lipsman et al., 2018; Mainprize et al., 2019; Rezai et al., 2020). While these agents primarily penetrate the brain via paracellular diffusion through the disrupted tight junctions, additional pathways such as receptor-mediated transcytosis and adsorptive endocytosis may also facilitate their transport (Burgess et al., 2015; Hawkins and Davis, 2005). Similarly, gadolinium-based contrast agents, which normally cannot cross an intact BBB, gain access through these temporary junctional openings and accumulate in brain tissue. This characteristic underpins the use of gadolinium-enhanced magnetic resonance imaging (MRI) as the standard method for detecting and confirming BBB opening in both research and clinical settings (McDannold et al., 2006). However, concerns regarding the safety of repeated gadolinium administration, including risks of nephrogenic systemic fibrosis and gadolinium retention in brain tissue, have prompted the development of contrast-free imaging methods to safely monitor BBB integrity over repeated treatments (Gulani et al., 2017; Kanda et al., 2014).

In addition to facilitating molecular delivery, focused ultrasound-induced BBB opening (FUS-BBBO) can modulate neural activity, triggering significant changes in brain functional connectivity

and neuroinflammation, as well as influencing behavior outcomes. For instance, studies in non-human primates have reported enhanced cognitive performance, including improved response speed and accuracy, following targeted striatal FUS-BBBO, indicating neuromodulatory effects beyond simple molecular delivery (Chu et al., 2015; Pouliopoulos et al., 2021; Todd et al., 2019). Functional MRI studies have demonstrated that FUS-BBBO can alter resting-state functional connectivity in both animals and humans, suggesting transient disruption of network dynamics (Meng et al., 2019; Todd et al., 2018). Notably, a recent non-human primate study compared the effects of FUS-neuromodulation and FUS-BBBO, showing that BBB opening alone can induce robust, region-specific changes in connectivity, further supporting a neuromodulatory role that does not depend on drug delivery (Liu et al., 2023). In parallel, FUS-BBBO has been shown to elicit transient neuroinflammatory responses, including glial activation, which may further contribute to downstream plasticity and behavioral effects (Kovacs et al., 2017; McMahon and Hynynen, 2017). Despite accumulating evidence of these neuromodulatory phenomena, the precise physiological mechanisms underlying these broader effects remain incompletely understood, necessitating deeper exploration into the cellular, molecular, and functional changes triggered by transient FUS-BBBO.

A key factor in maintaining neurovascular homeostasis, which may potentially be involved in the neuromodulatory effects of FUS-BBBO, is the regulation of water transport across the BBB. Aquaporin-4 (AQP4), a water channel protein abundantly expressed on astrocytic endfeet at the gliovascular interface, facilitates water exchange in response to osmotic and hydrostatic gradients, modulating cerebral edema, neuroinflammation, and glymphatic clearance (Papadopoulos and Verkman, 2013). Given its small molecular size (~18 Da), water acts as a highly sensitive endogenous tracer, capable of detecting subtle permeability alterations that larger molecules such as gadolinium (~550 Da) might fail to reveal (Dickie et al., 2020; Shao et al., 2020; Uchida et al., 2023). Thus, studying water transport dynamics offers an exceptionally sensitive and

physiologically relevant avenue to detect and better understand subtle BBB permeability and functional changes induced by FUS-BBBO.

Diffusion-prepared pseudo-continuous arterial spin labeling (DP-pCASL) is a recently developed, non-invasive MRI technique to quantify the water exchange rate (K_w) across the BBB. By combining diffusion weighting with ASL and employing multi-post-labeling delay acquisitions, DP-pCASL improves K_w accuracy by accounting for arterial transit time (ATT) variability (Shao et al., 2019; St. Lawrence et al., 2012; Wang et al., 2007). Clinical studies have reported changes of BBB K_w in association with aging (Shao et al., 2024) and various neurological conditions, including multiple sclerosis (Wengler et al., 2020), obstructive sleep apnea (Palomares et al., 2015) and cerebral small vessel disease (Li et al., 2023). In Alzheimer's disease, Chen et al. reported significantly reduced K_w in the hippocampus, cingulate cortex, and other brain regions, with associations to plasma biomarkers and cognitive performance, suggesting K_w as a promising biomarker for early BBB dysfunction (Chen et al., 2025). Additionally, Tiwari et al. demonstrated the sensitivity of diffusion-weighted ASL MRI to mannitol-induced BBB disruption in rodents, validated by contrast-enhanced MRI and histology (Tiwari et al., 2025).

Despite these methodological advancements, DP-pCASL has not yet been applied to characterize the changes in water exchange dynamics associated with FUS-induced BBB opening. The aim of the present study, therefore, is to quantify alterations in cerebral blood flow (CBF) and BBB water exchange rate (K_w) following FUS-BBBO targeting the dorsal striatum of non-human primates (NHPs) (**Figure 1**). By directly comparing these gadolinium-free DP-pCASL measures with conventional gadolinium-enhanced MRI, we seek to evaluate the potential of DP-pCASL as a non-contrast imaging approach for assessing BBB permeability and to gain insight into the mechanisms by which focused ultrasound transiently alters BBB integrity.

Materials and Methods

Animal Preparation

Four adult male NHPs, 2 long-tailed macaques (*Macaca fascicularis*) and 2 rhesus macaques (*Macaca mulatta*), weighing between 7.1 and 14.1 kg, were included in this study. Prior to the ultrasound and MRI procedures, animals were initially sedated with ketamine (10 mg/kg) and dexmedetomidine (0.02 mg/kg). Anesthesia was then maintained with inhaled isoflurane at concentrations ranging from 0.8% to 1.1% throughout the experiments. The scalp hair was shaved, and a conductive gel was applied to optimize acoustic coupling for ultrasound delivery. During MRI scanning, physiological parameters—including body temperature, electrocardiogram, oxygen saturation, and end-tidal CO_2—were continuously monitored using a wireless MRI-compatible system (Iradimed 3880). To minimize potential confounding effects from repeated anesthesia and to ensure complete restoration of BBB integrity between experiments, a strict wash-out period was enforced. Specifically, the interval between consecutive MRI sessions for each subject was maintained at a minimum of 10 days. This duration significantly exceeds the typical 48–72 hour window required for BBB closure and functional recovery in non-human primates (Marquet et al., 2014; Pouliopoulos et al., 2021). Consequently, the frequency of scanning was limited to no more than two sessions per month per animal. All experimental protocols were conducted in accordance with guidelines approved by the Institutional Animal Care and Use Committee (IACUC) of Columbia University.

FUS with microbubbles application

A single-element FUS transducer (model H-107; 500 kHz frequency; radius of curvature 63.2 mm; outer diameter 64 mm; Sonic Concepts, Bothell, WA) was used for all sonication. The transducer

was driven by a function generator (Agilent 33220A, Agilent Technologies, Santa Clara, CA) connected to a 57 dB radiofrequency power amplifier (500S06, E&I, Rochester, NY). The transducer's acoustic output was calibrated in a degassed water tank using a capsule hydrophone (HGL-0200, Onda Corp., Sunnyvale, CA), which measured free-field pressure, focal location, and acoustic intensities including spatial-peak pulse average (I_{sppa}) and spatial-peak temporal average (I_{spta}). To estimate the actual acoustic pressure reaching the brain, attenuation through *ex vivo* NHP skulls was measured. To estimate the in situ acoustic pressure, we considered a transcranial attenuation range of 60–65% due to the skull, a value consistent with previous numerical and experimental characterizations (T. Deffieux and E. E. Konofagou, 2010; Wu et al., 2018). In this study, we adopted a conservative 65% reduction to report the derated peak negative pressure (PNP), thereby accounting for potential losses due to skull heterogeneity and incidence angles.

On the day of MRI scanning, the transducer cone was filled with degassed water using a WDS105+ water degassing system (Sonic Concepts, Bothell, WA) and attached securely to the NHP's scalp to optimize ultrasound transmission. Sonication parameters were based on established protocols to safely and effectively induce BBB opening in NHPs. Animals received sonication for 2 minutes at a derated PNP of 400 kPa, with a pulse repetition frequency (PRF) of 2 Hz, pulse duration of 10 ms, and a 2% duty cycle, as illustrated in **Figure 2**. In-house manufactured microbubbles (lipid-shelled with a perfluorobutane core; diameter 4–5 μm; concentration 2.5×10^8 bubbles/kg) were prepared and stored at 4°C following established protocols (Feshitan et al., 2009; Tung et al., 2011). On the day of the experiment, microbubbles were activated via mechanical agitation immediately prior to use. They were administered as a bolus injection intravenously via the saphenous vein approximately 10 seconds after the start of sonication (injection duration < 10 s). The spatial peak temporal average intensity (Ispta) for BBB opening was 39.2 mW/cm^2. This ultrasound intensity was selected to reliably open the BBB while maintaining safety, as supported by prior studies(Liu et al., 2023; Pouliopoulos et al., 2021).

MRI Acquisition

MRI data were acquired on a 3T Siemens Prisma scanner using a 15-channel knee coil optimized for imaging the NHP brain, and the detailed MRI timeline is shown in **Figure 2**. Structural T1-weighted images were obtained using a T1-MPRAGE sequence with the following parameters: repetition time (TR) = 2580 ms, echo time (TE) = 2.81 ms, inversion time (TI) = 1160 ms, flip angle (FA) = 9°, isotropic resolution of 0.5 mm^3, and field of view (FOV) = 128 × 128 × 120 mm^3.

DP-pCASL with background-suppressed 3D gradient-and-spin-echo (GRASE) readout was performed within 45 minutes after FUS sonication to measure ATT, CBF, and the BBB K_w, following a protocol similar to that described by Shao et al. (Shao et al., 2019). The detailed parameters included: field of view (FOV) = 138 mm, matrix size = 64 × 64, 14 axial slices, voxel size = 2.2 × 2.2 × 5 mm^3, turbo factor = 14, EPI factor = 64, bandwidth = 2232 Hz/pixel, TE = 31.84 ms, TR = 3200 ms, labeling/control duration = 1000 ms, labeling offset = 55 mm, and centric k-space ordering. Multiple post-labeling delays (PLDs) (600, 1400 and 1700 ms) were acquired with diffusion weightings (b-values) applied to capture water exchange dynamics.

To confirm FUS-mediated BBBO, T1-weighted images were acquired using a T1-SPACE protocol, selected for its sensitivity to low gadolinium concentrations (Danieli et al., 2019), within 20 minutes following intravenous administration of gadolinium-based contrast agent at a dose of 0.2 mmol/kg. The T1-SPACE images matched the pre-contrast T1 and resolution to enable direct comparison.

MR Image Analysis

A two-stage estimation approach was used to quantify CBF, ATT and BBB K_w from perfusion images acquired at specific post-labeling delays (PLD) and diffusion weightings (b-values) (St.

Lawrence et al., 2012), as described in **Figure 3**. In the first stage, ATT was estimated using the flow-encoding arterial spin tagging (FEAST) method, calculated from the ratio of vascular-suppressed signals (with diffusion weighting = 10 s/mm² and velocity encoding [VENC] = 7.5 mm/s) to the total perfusion signals acquired at a short PLD of 600 ms (Wang et al., 2003). In the second stage, K_w was calculated by fitting data acquired at two longer PLDs of 1,400 ms and 1,700 ms with diffusion weightings of b = 0 and 25 s/mm², which allows separation of vascular and extravascular compartments using a two-compartment single-pass approximation (SPA) model (Shao et al., 2019; St. Lawrence et al., 2012). CBF was computed from perfusion signals measured at PLD = 1,700 ms without diffusion weighting (Alsop et al., 2015).

For localized quantitative analysis, specific regions of interest (ROIs) were defined on the single axial slice intersecting the dorsal striatum, selected from the limited field-of-view ASL acquisition. The planned target ROI, serving as the primary anatomical reference, was manually delineated directly on the parametric maps. Each ROI covered a 2 × 2 × 1 voxel volume (4.4 × 4.4 × 5 mm³), centered on the dorsal caudate nucleus as identified on the corresponding T2-weighted structural scan acquired at the same slice plane. The control ROI was defined by mirroring this planned target ROI to the contralateral hemisphere. To independently validate the targeting accuracy and characterize the physiological extent of the functional opening, a complementary Gd-defined target ROI was generated through a multi-step image processing pipeline. Difference maps were generated by subtracting pre-contrast T1-weighted images from post-contrast images. A signal intensity threshold was then applied (defined as the mean intensity of the difference map plus 2 × standard deviation) to identify enhancement. We manually removed artifacts arising from hyper-intense vessels and ventricular spaces to isolate tissue-specific extravasation, and the resulting mask was smoothed with a Gaussian kernel ($\sigma = 1$) to ensure spatial continuity. To account for inter-scan physiological variations, voxel-wise K_w values were normalized to the global 98th percentile value.

To verify the spatial consistency between the planned and Gd-defined target definitions, we assessed the distribution of water exchange rates across the different region types. The normalized voxel-wise values were compared across the control, planned target, and Gd-defined target groups using a one-way analysis of variance (ANOVA) followed by Welch's t-tests for pairwise comparisons.

Comprehensive assessment of the FUS-BBBO effect was performed at the group level using permutation testing. For global physiological changes, whole-brain average values of CBF, ATT, and K_w were compared between non-BBBO (n = 6) and BBBO (n = 7) sessions using two-tailed independent-samples permutation tests in MATLAB R2023a (The MathWorks, Natick, MA, USA). Concurrently, the specific local treatment effect was evaluated by comparing the mean parameter values within the planned target ROI (BBBO) against the contralateral ROI (control) using paired-sample permutation testing. All permutation analyses utilized 10,000 iterations to determine statistical significance, with mean difference (Δ), p-value, and Hedges' g reported. All co-registration and ROI operations were performed in FSL v6.0 (FMRIB Software Library, University of Oxford, Oxford, UK) (Jenkinson et al., 2012), with statistical significance defined at $p < 0.05$.

Results

Mapping of CBF, ATT, and K_w and its relation to contrast-enhanced T1

We first tested the effect of FUS-BBBO on hemodynamics and BBB water exchange. **Figure 4A** shows voxel-wise maps of CBF, ATT, and BBB K_w in the axial plane through the dorsal striatum for two representative BBBO sessions in NHPs T and R. Both sessions targeted the right caudate and were acquired immediately after sonication with microbubbles. The CBF maps illustrate the baseline perfusion pattern throughout the striatum, with no systematic ipsilateral-to-contralateral

differences attributable to BBBO. ATT maps display considerable variability across individual sessions, with average ATT values ranged from 918 to 1288 ms; however, there is no clear spatial correspondence between ATT heterogeneity and the BBBO locus. By contrast, K_w maps reveal pronounced, spatially restricted reductions in water-exchange rate at or immediately adjacent to the sonication site (white arrows), highlighting the unique sensitivity of K_w to focal BBB permeability changes. Furthermore, visual inspection of the raw EPI and structural T1-weighted images revealed no signs of macroscopic hemorrhage or edema in the sonicated regions, suggesting that the observed changes in water exchange rates were not confounded by tissue lesions.

The spatial specificity of the observed K_w changes was verified by cross-referencing the functional maps with anatomical BBB opening. Figure 4B presents the multi-planar anatomical verification for a representative session, where comparison between the pre- and post-contrast T1-weighted images revealed a distinct, focal hyperintense region in the dorsal striatum. This confirmed successful contrast agent extravasation. The segmentation analysis demonstrated that the contrast-enhanced region (red mask) aligned precisely with the manually defined planned target ROI (white box), while the contralateral control ROI (green box) remained devoid of enhancement. To further validate K_w as a potential biomarker, we superimposed the K_w maps onto the high-resolution T1-weighted images. As illustrated in the zoomed-in panels of Figure 4C, the region of reduced K_w (blue overlay) exhibited excellent spatial concordance with the Gd-enhancement pattern. The reduction in water exchange rate was strictly confined to the sonicated area, establishing a direct link between BBB disruption and the local decrease in K_w.

Quantitative analysis further confirmed a robust reduction in water exchange rates within the targeted regions. The control ROI exhibited a minor baseline deviation of -5.52% ± 2.62% relative to the global maximum, reflecting normal tissue heterogeneity. In contrast, the primary planned target ROI showed a substantial reduction of -16.39% ± 1.09%. Importantly, the complementary

analysis using the Gd-defined ROI yielded a highly consistent reduction of -14.47% ± 1.68%. Statistical analysis revealed a significant difference between groups (one-way ANOVA, $p < 0.001$). Post-hoc tests confirmed that both the planned target and Gd-defined target groups differed significantly from the control group ($p < 0.001$), with large effect sizes (Cohen's d values are 5.42 and 4.09 respectively). The statistical consistency between the geometrically planned target and the functionally defined Gd-mask confirms that the observed K_w reduction is a robust physiological effect, independent of the specific ROI definition method employed.

Group-level comparison of whole-brain averages

To assess the reproducibility of BBBO effects, whole-brain CBF, ATT, and K_w were compared across four NHPs (non-BBBO: 6 sessions; BBBO: 7 sessions) via non-parametric permutation tests (**Figure 5A**). Whole-brain CBF showed no significant change following BBBO, with median (IQR) values of 31.3 (22.5–36.5) $\mathrm{ml} \cdot 100\ \mathrm{g}^{-1} \cdot \mathrm{min}^{-1}$ in non-BBBO versus 29.3 (22.2–33.0) $\mathrm{ml} \cdot 100\ \mathrm{g}^{-1} \cdot \mathrm{min}^{-1}$ in BBBO; permutation testing (10 000 iterations) yielded $p = 0.64$, a mean $\Delta = -3.0\ \mathrm{ml} \cdot 100\ \mathrm{g}^{-1} \cdot \mathrm{min}^{-1}$, and Hedges' $g = -0.25$. Whole-brain ATT shifted from a median (IQR) of 1204 (931–1264) ms in non-BBBO to 989 (930–1042) ms in BBBO; despite this apparent decrease, permutation testing (10 000 iterations) indicated no significant effect ($p = 0.22$; mean $\Delta = -106.9\ \mathrm{ms}$; Hedges' $g = -0.65$). In contrast, whole-brain K_w increased significantly after BBBO, with median (IQR) values of 49.8 (46.3 - 55.9) min^{-1} in non-BBBO versus 59.4 (56.6 - 66.3) min^{-1} in BBBO; permutation testing (10, 000 iterations) yielded $p < 0.01$, a mean $\Delta = 13.6\ \mathrm{min}^{-1}$ and Hedges' $g = 1.46$, indicating a diffuse enhancement of water-exchange rate across the brain.

ROI analysis between BBBO site and contralateral control

To assess focal effects of BBBO, CBF, ATT, and K_w were compared within the caudate ROI (planned target) at the BBBO site versus the mirrored contralateral control (n = 7 sessions) using two-tailed paired permutation tests (10,000 iterations; **Figure 5B**). CBF showed no significant change following BBBO, with median values of 31.3 (24.7- 32.0) $\mathrm{ml} \cdot 100\,\mathrm{g}^{-1} \cdot \mathrm{min}^{-1}$ in the contralateral control versus 32.0 (29.3 – 34.7) $\mathrm{ml} \cdot 100\,\mathrm{g}^{-1} \cdot \mathrm{min}^{-1}$ in the BBBO ROI; permutation testing yielded p = 0.46, a mean Δ = 3.4 $\mathrm{ml} \cdot 100\,\mathrm{g}^{-1} \cdot \mathrm{min}^{-1}$, and Hedges' g = 0.27. ATT likewise showed no significant change, with median values of 1034.9 (972.5 – 1131.5) ms in control versus 989.6 (887.9 - 1120.9) ms in BBBO (p = 0.58; mean Δ = -30 ms; Hedges' g = -0.17). K_w decreased significantly at the BBBO site, with median values of 61.6 (58.3 – 70.4) min^{-1} in control versus 45.0 (40.6 – 55.6) min^{-1} in BBBO; permutation testing yielded $p < 0.05$, a mean Δ = -15.7 min^{-1} and Hedges' g = -1.51, indicating a localized suppression of water-exchange rate at the sonication locus.

Discussion

This study demonstrates that FUS combined with microbubbles significantly reduces BBB K_w in the dorsal striatum of non-human primates. By contrast, our between-group analysis showed that whole-brain K_w was significantly higher in BBBO cases than in non-BBBO controls. The local reduction in K_w is consistent with a recent rodent study by Tiwari et al. (Tiwari et al., 2025), which used diffusion-weighted ASL MRI to assess BBB water exchange following chemically induced disruption and reported significantly reduced K_w in the affected hemisphere. Similar reductions in K_w have also been reported in individuals with neurological conditions such as aging, Alzheimer's disease, and cerebrovascular disorders, where impaired BBB function has been frequently reported. (Chen et al., 2025; Palomares et al., 2015; Uchida et al., 2023; Wengler et al., 2020). Together, these converging results suggest that reduced K_w may serve as a common physiological signature of compromised BBB function, whether induced by external interventions or underlying disease, and support its application in evaluating the impact of FUS-BBBO.

The focal reduction in BBB K_w observed after FUS-BBBO suggests underlying cellular and molecular adaptations in response to barrier disruption. Aquaporin-4 (AQP4) water channels, primarily located on astrocytic endfeet, are key regulators of cerebral water homeostasis and glymphatic clearance (Mestre et al., 2018; Papadopoulos and Verkman, 2013). FUS-induced loosening or disruption of tight junctions may activate signaling pathways that alter AQP4 expression or polarization—potentially as a protective mechanism to regulate transvascular water flux and limit vasogenic edema (Cong and Kong, 2020). Similar regulatory responses have been reported in neuropathological conditions associated with BBB dysfunction, such as Alzheimer's disease, stroke, and traumatic brain injury (Hirt et al., 2017; Tang et al., 2014; Zeppenfeld et al., 2017). Therefore, a reduction in K_w at the FUS-sonicated area may reflect an active homeostatic adjustment rather than a passive increase in permeability or leakage.

Moreover, our studies align with a growing consensus that BBB permeability is a dynamic, multifactorial phenomenon rather than a mere consequence of tight-junction disruption (Daneman and Prat, 2015; Sweeney et al., 2018). Endothelial remodeling, including changes in cell shape, junctional protein expression and transporter activity, pericyte detachment or loss, and astrocyte endfoot reactivity all modulate paracellular and transcellular flux (Abbott et al., 2006; Armulik et al., 2011). In parallel, neuroinflammatory mediators (e.g. IL-1β, TNF-α, matrix metalloproteinases, reactive oxygen species) and glymphatic flow disturbances each contribute to net water and solute exchange across the barrier (Kovacs et al., 2017; Mestre et al., 2018). By capturing the rapid FUS-induced changes in BBB K_w of non-human primates, DP-pCASL provides a single quantitative measure that integrates the net effects of endothelial remodeling, astrocyte reactivity, and inflammatory signaling on BBB water exchange (Kovacs et al., 2017; Shao et al., 2019).

In this study, we also observed a significant increase in the whole-brain K_w following FUS-BBBO targeted to the caudate nucleus. While the underlying mechanism remains unclear, a recent study has linked elevated whole brain K_w to improved executive function in older adults (Pappas et al., 2024). Although our study did not directly assess cognitive function after BBBO, earlier work has shown that FUS-BBBO can enhance visual behavior task performance in non-human primates by improving both accuracy and response speed, suggesting a potential neuromodulatory effect accompanying BBBO (Chu et al., 2015; Downs et al., 2017). Furthermore, recent work has demonstrated that FUS-BBBO in the dorsal striatum can activate broader brain networks including the default mode network and frontotemporal network (Liu et al., 2023). These findings raise the possibility that global K_w increases may reflect broader functional shifts in neurovascular regulation or fluid transport pathways beyond the sonicated target.

The observed K_w values in NHPs (median whole-brain average are 49.8 min^{-1} and 59.4 min^{-1} for non-BBBO and BBBO conditions respectively) are lower than those typically reported in awake humans (~100-120 min^{-1}). This discrepancy likely arises from the systemic effects of isoflurane

anesthesia, which is known to alter cerebral blood flow, metabolism, and neurovascular coupling, as well as the use of different anesthetic protocols in NHP versus awake human studies (Li et al., 2014; Slupe and Kirsch, 2018; Zhang, 2022). In addition, ASL-based estimates of the BBB water exchange rate K_w have previously been shown to vary across species and experimental conditions, with animal studies often reporting different values with those in humans and attributing these differences to species-dependent capillary surface area, anesthesia, and modeling choices (Shao et al., 2023; Tiwari et al., 2017). Finally, imaging of the smaller NHP brain is more susceptible to partial volume effects compared to human studies, presenting a challenge for the precise quantification of ASL-derived kinetic parameters like K_w (Asllani et al., 2008; Chappell et al., 2021). However, to the best of our knowledge, this is the first study to quantify BBB water exchange rates in non-human primates using DP-pCASL. Therefore, these findings provide a critical baseline for future preclinical investigations into BBB permeability dynamics.

This study also investigates the potential of DP-pCASL as a non-invasive, contrast-free imaging biomarker for monitoring FUS-induced BBB permeability. Currently, dynamic contrast enhanced MRI (DCE-MRI) is widely used to evaluate BBB integrity by measuring the leakage of contrast agents (CA) into the tissue's interstitial space, indicated by increased T1-weighted signal intensity. Using pharmacokinetic model computations, the volume transfers constant K^{trans} serves as a surrogate measure of BBB permeability (Sourbron and Buckley, 2013). However, the safety of exogenous parametric CA (i.e. Gadolinium) has become a concern for human health (Gulani et al., 2017; Harvey et al., 2020). Recent research has focused on non-Gd-based methods for imaging the BBB integrity, including the use of D-glucose as a CA for chemical exchange saturation transfer (CEST) MRI (Xu et al., 2015), and arterial spin labeling (ASL) for measuring water exchange as a marker for non-contrast detection of BBB impairment (Li et al., 2022). Diffusion tensor imaging (DTI) has been investigated as a non-contrast method for BBB opening detection, linking changes in fractional anisotropy to BBB permeability (Karakatsani et al., 2020).

However, DTI provides no direct hemodynamic or perfusion metrics, such as cerebral blood flow or volume, that are more physiologically tied to barrier function (Le Bihan and Iima, 2015). In contrast, DP-pCASL specifically quantifies BBB water exchange rates by differentiating labeled water in vascular and extravascular compartments using diffusion weighting and kinetic modeling (Shao et al., 2019; St. Lawrence et al., 2012). This provides a direct and physiologically meaningful measurement of BBB permeability to water, an endogenous tracer with small molecular size and ubiquitous presence.

This study did not reveal sustained or statistically significant changes in CBF or ATT at either the whole-brain level or within the BBBO ROI. Although Labriji et al. (2023) reported a 29.6 ± 15.1 % decrease in CBF and prolonged ATT following BBBO in rats (Labriji et al., 2023), our NHP data showed only modest, non-significant fluctuations (whole-brain CBF $\Delta = -3.0$ mL·100 $g^{-1}\cdot min^{-1}$; $p = 0.64$; whole-brain ATT $\Delta = -106.9$ ms; $p = 0.22$). These discrepancies may reflect differences in BBBO targeting and volume, species differences (earlier study in rodents versus our work in non-human primates), and the limited longitudinal sampling in our current protocol, which may have missed the critical timeline of CBF drops (Rigollet et al., 2024). Additionally, isoflurane anesthesia, a potent cerebral vasodilator, likely alters vascular responsiveness during these experiments, thereby masking subtle changes induced by BBBO and further limiting CBF and ATT as reliable, noninvasive biomarkers of BBBO in NHPs (Slupe and Kirsch, 2018).

It is worth noting that the observed whole-brain CBF range of 14.7 - 54.9 ml/100g/min is broadly consistent with the physiological range reported in a recent NHP pCASL study by Johnson et al., which documented a baseline whole-brain CBF range of 21.47 - 77.23 ml/100g/min (Johnson et al., 2024). While the median values in present study (31.3 ml/100g/min and 29.3 ml/100g/min for non-BBBO and BBBO conditions respectively) are lower than their reported mean (~51.5 ml/100g/min), this difference can be contributed to the dose-dependent vasodilator effect of isoflurane (Li et al., 2014). Specifically, a lower maintenance concentration was used in the

current protocol (0.8–1.1%) compared to the 1.5% employed by Johnson et al. Notably, the measurements align closely with gold-standard PET values obtained under propofol anesthesia which reported a whole brain CBF range of 23 - 42 ml/100g/min (Kudomi et al., 2005). Furthermore, while earlier studies using continuous ASL reported much higher CBF (~104 ml/100g/min in grey matter)(Zhang et al., 2007), those elevations may be attributable to methodological differences inherent to continuous labeling techniques coupled with deeper anesthesia.

The study has several limitations. First, the spatial resolution is primarily constrained by the signal-to-noise ratio (SNR), which is influenced by acquisition time and coil sensitivity. Consequently, scattered low K_w regions located near the brain edges, ventricles, and sulci likely reflect inherent signal fluctuations and partial volume effects. However, within the brain parenchyma, the region of reduced K_w extended beyond the boundaries of Gd-enhanced region, Given the differential sensitivity between water (~18 Da) and gadolinium-based contrast agents (~550 Da), it is biologically plausible that FUS induces functional alterations in water dynamics in peripheral areas where the barrier is modulated but not physically disrupted enough to leak contrast agent. Additionally, we cannot rule out that some remote changes represent genuine physiological modulation coupled with functional network shifts (Liu et al., 2023), although characterizing these distinct physiological fluctuations remains a subject for future investigation. To overcome these current resolution limits, recent motion-compensated, multi-delay diffusion-weighted ASL with isotropic 3.5 mm^3 resolution in humans (Shao et al., 2023) may substantially improve both sensitivity and resolution.

Second, DP-pCASL was acquired at approximately 45-60 min post-sonication, capturing only offline effects rather than the full opening–recovery time course. Longitudinal, multi-time point imaging will be essential to elucidate how FUS-BBBO dynamically alters cerebral blood flow and water-exchange metrics over time (Labriji et al., 2023; Rigollet et al., 2024; Sun et al., 2015).

Third, potential limitations related to repeated isoflurane anesthesia and the absolute Kw value must be carefully considered. While K_w is highly sensitive to changes in BBB permeability, the absolute K_w values reported in this study, which were obtained under isoflurane anesthesia, may not perfectly reflect the values of an awake NHP due to the systemic effects of volatile agents (Slupe and Kirsch, 2018). However, in the context of this within-subject design focusing on changes, the stability of CBF and ATT (systemic and anesthesia-sensitive metrics) across sessions strongly suggests that the observed increase in K_w is not caused by a general cumulative systemic effect (e.g., gradual shift in vascular tone or ETCO2 drift). Instead, the change in K_w is more likely attributed to the targeted BBBO procedure itself and its interaction with global brain networks.

Fourth, our single-pass approximation kinetic model simplifies the microvascular environment and does not fully capture transcellular water movement through AQP4 channels or intra-voxel transit-time heterogeneity. While we accounted for voxel-wise arterial transit time (ATT) in this study, further refinements could incorporate mechanisms suggested by recent multi-echo time ASL studies, such as using varying echo times to probe AQP4-associated transcellular flux (Ohene et al., 2019), or modeling intra-voxel transit-time dispersion to improve estimation accuracy (Mahroo et al., 2021). Incorporating these advanced models and validating the resulting K_w values against dynamic contrast-enhanced MRI–derived K^{trans} measurements (Hývlová et al., 2025; Tiwari et al., 2025; Vlachos et al., 2010) could enable precise mapping of how FUS affects both the timing and spatial distribution of transcellular and paracellular water exchange.

In conclusion, our findings demonstrate that FUS-mediated BBB opening results in decreased K_w at the focal site alongside a global increase in whole-brain K_w, revealing complex physiological adaptations that can be noninvasively monitored using DP-pCASL. This technique offers a safe, repeatable, and sensitive tool for detecting and tracking BBB permeability changes, with strong potential for both preclinical research and clinical application in neurotherapeutics.

Credit author statement

D.L. and V.P.F. designed the study, collective and analyzed the data and wrote the manuscript. X.S. and D.J.J.W. provided critical support for implementing the DP-pCASL sequences and processing the data. R.L. configured the MRI sequence and assisted with data collection. F.M. and S.S. helped with study design, device calibration, and data collection. E.E.K. provided focused ultrasound expertise. V.P.F. and E.E.K. supervised the study.

Acknowledgements

The authors wish to acknowledge the ZI-ICM team for the setup and anesthesia procedures during MRI imaging, and ZI-MRI team for the MRI sequence setup and data collection. The work was supported by NIH R01 MH133020 (V.P. Ferrera and E.E. Konofagou), R01 NS134712 (D.J.J. Wang) and BBRF Young Investigator grant 31298 (D. Liu).

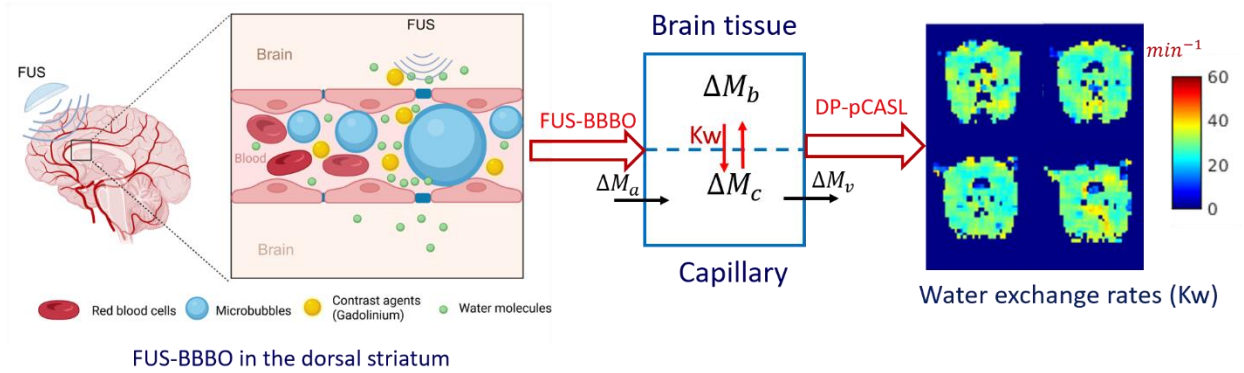

Figure 1 Schematic pipeline for measuring blood–brain barrier (BBB) water exchange between capillary and brain tissue using diffusion-prepared pseudo-continuous arterial spin labeling (DP-pCASL) after focused ultrasound (FUS)–mediated BBB opening in non-human primates (NHPs). Part of the figure was created using BioRender.com. ΔM_a, ΔM_b, ΔM_c and ΔM_v represent the magnetization of labeled water in the arterial, brain tissue, capillary, and venous compartments, respectively. K_w denotes the water exchange rate across BBB.

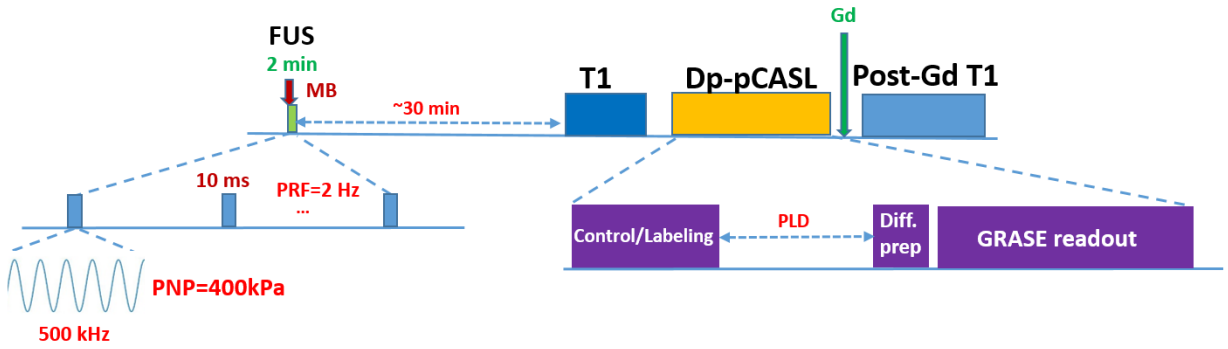

Figure 2 FUS procedures and MRI acquisition: A 2-min focused ultrasound (FUS) exposure combined with microbubbles (MB) was followed by MRI scans, including T1, diffusion-prepared pCASL (2.2 × 2.2 × 5 mm^3 resolution, 600-1700 ms post-labeling delays (PLDs), with diffusion weighted), and a post-Gadolinium T1 scan to confirm blood-brain barrier (BBB) opening.

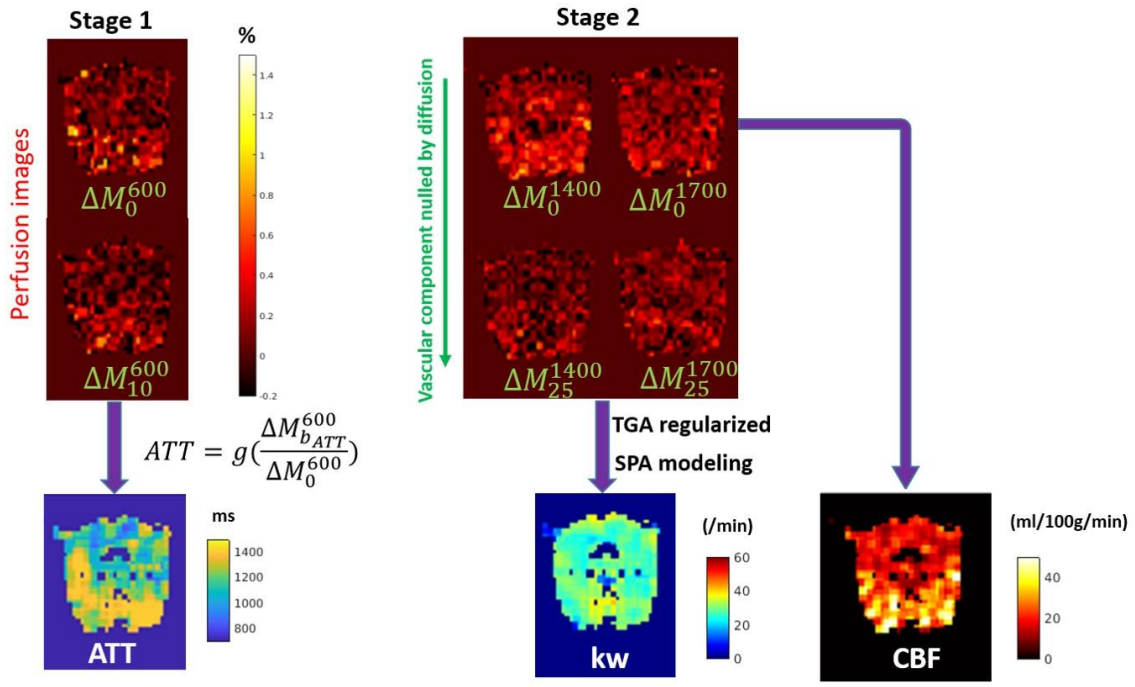

Figure 3 Two-stage estimation of arterial transit time (ATT), water-exchange rate (K_w), and cerebral blood flow (CBF). ATT is estimated via FEAST using the ratio of diffusion-weighted (b_{ATT} = 10 s/mm²) to non-weighted ASL signal at post-labeling delay (PLD) = 600 ms. K_w is derived from the two-compartment single-pass approximation model fitted to DP-pCASL data. CBF is calculated from ΔM_0^{1700} (b = 0 s/mm², PLD = 1700 ms) without diffusion preparation. Here, ΔM_b^{PLD} denotes the ASL difference signal with diffusion weighting b and delay PLD.

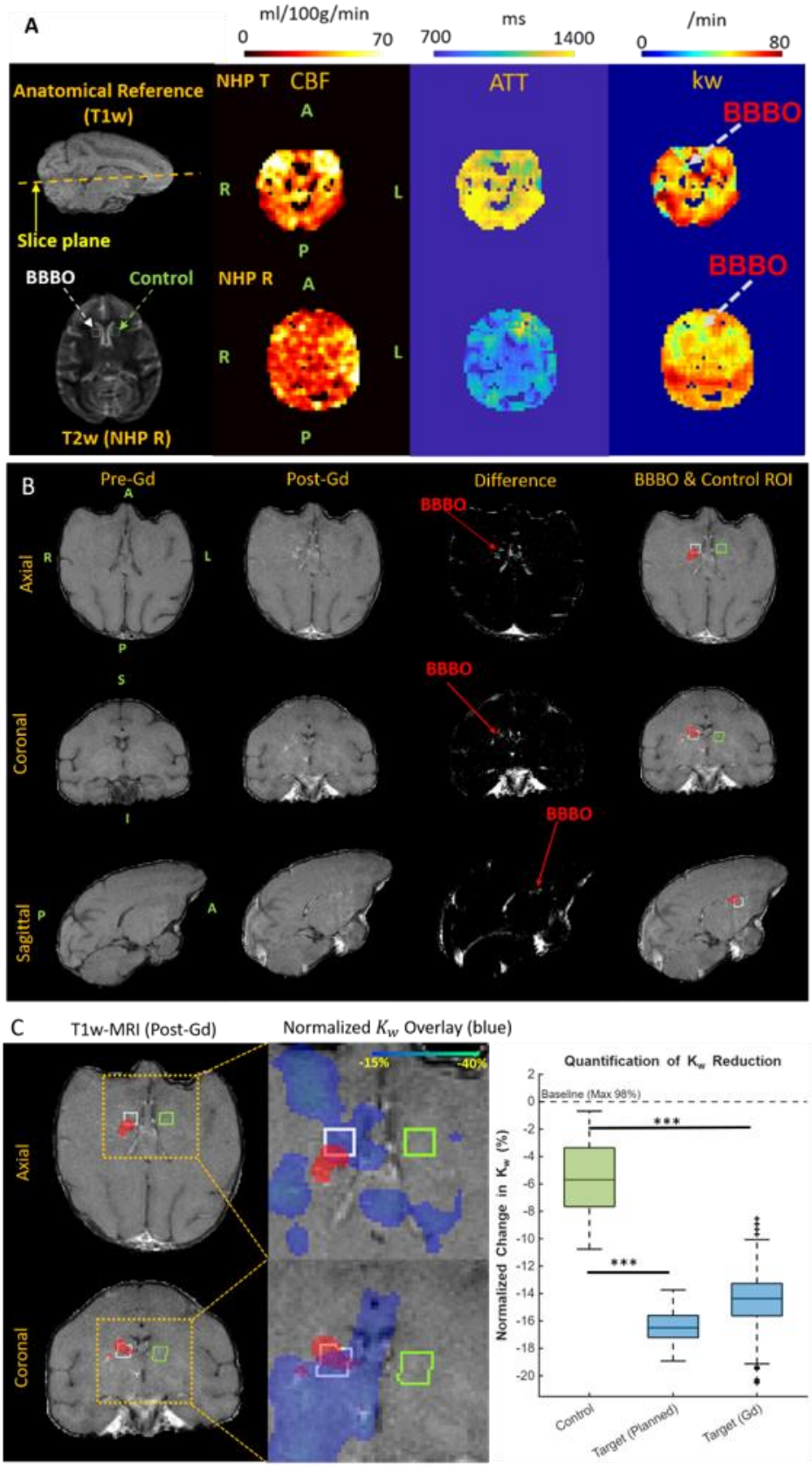
A
ml/100g/min
0
70
ms
700
1400
/min
0
80
Anatomical Reference (T1w)
Slice plane
BBBO
Control
T2w (NHP R)
NHP T
CBF
ATT
kw
BBBO
NHP R
A
R
L
P
B
Pre-Gd
Post-Gd
Difference
BBBO & Control ROI
Axial
Coronal
Sagittal
S
I
C
T1w-MRI (Post-Gd)
Normalized K_w Overlay (blue)
-15%
-40%
Quantification of K_w Reduction
Baseline (Max 98%)
Normalized Change in K_w (%)
***
Control
Target (Planned)
Target (Gd)

487

Figure 4. Spatial specificity of FUS-induced BBBO and cross-validation of K_w changes. (A) Representative parametric maps from NHPs R and T following FUS targeting the right caudate. Left column (Anatomical Reference) shows sagittal scouts indicating the ASL slice (yellow dashed line) and axial T2 images with planned target and contralateral control ROIs (square outlines). Subsequent columns show CBF, ATT, and K_w maps. Arrows and "BBBO" labels indicate focal K_w reduction within the sonicated region. (B) Anatomical verification. The Gd-defined target ROI (red mask) was generated from the difference between post- and pre-contrast T1 images, followed by thresholding, artifact removal, and smoothing. This overlay illustrates the spatial relationship between Planned Target (white box), Gd-defined Target (red mask), and Control (green box) ROIs. (C) Functional-anatomical concordance. Left: Zoomed overlay of K_w on T1 demonstrates specific K_w reduction (blue) within the Gd-enhanced BBBO region. Right: Quantitative comparison of normalized voxel-wise K_w across Control, Planned, and Gd-defined targets. ANOVA followed by Welch's t-tests, reveals significant reductions in both targets vs. control, with highly consistent distributions between planned and Gd-defined targets ($p < 0.001$).

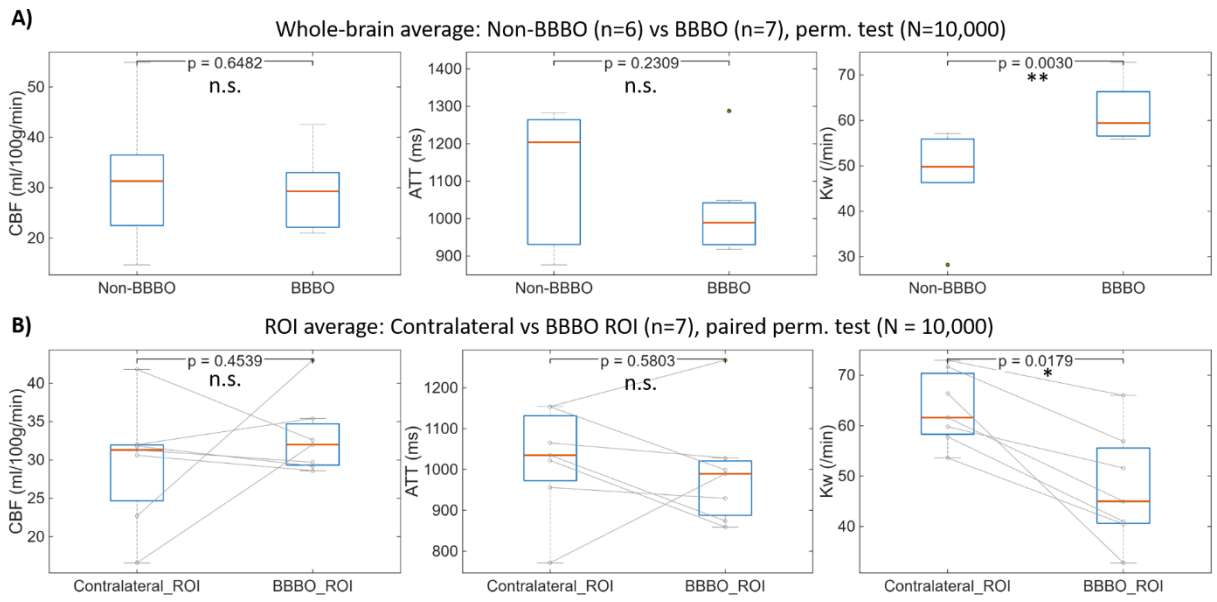

Figure 5 A) Whole-brain averages of cerebral blood flow (CBF), arterial transit time (ATT), and BBB water exchange rate (K_w) in non-BBBO (n = 6 sessions, 4 NHPs) and FUS-BBBO conditions (n = 7 sessions, 4 NHPs). Permutation tests (N = 10,000) showed no significant differences in CBF and ATT ($p > 0.05$), but a significant increase in whole-brain K_w following BBBO ($p < 0.01$). B) ROI analysis comparing the BBBO site (caudate) and the contralateral control region within the same sessions revealed a significant reduction in K_w at the BBBO site ($p < 0.05$, paired permutation test), while CBF and ATT showed no significant differences ($p>0.05$). All box plots display the median, 25th and 75th percentiles (box edges), and individual outliers.

References

Abbott, N.J., Rönnbäck, L., Hansson, E., 2006. Astrocyte–endothelial interactions at the blood–brain barrier. Nature Reviews Neuroscience 7, 41-53.

Alsop, D.C., Detre, J.A., Golay, X., Günther, M., Hendrikse, J., Hernandez‐Garcia, L., Lu, H., MacIntosh, B.J., Parkes, L.M., Smits, M., 2015. Recommended implementation of arterial spin‐labeled perfusion MRI for clinical applications: a consensus of the ISMRM perfusion study group and the European consortium for ASL in dementia. Magnetic resonance in medicine 73, 102-116.

Armulik, A., Genové, G., Betsholtz, C., 2011. Pericytes: developmental, physiological, and pathological perspectives, problems, and promises. Developmental cell 21, 193-215.

Aryal, M., Arvanitis, C.D., Alexander, P.M., McDannold, N., 2014. Ultrasound-mediated blood–brain barrier disruption for targeted drug delivery in the central nervous system. Advanced Drug Delivery Reviews 72, 94-109.

Asllani, I., Borogovac, A. and Brown, T.R., 2008. Regression algorithm correcting for partial volume effects in arterial spin labeling MRI. Magnetic Resonance in Medicine 60(6), 1362-1371.

Burgess, A., Shah, K., Hough, O., Hynynen, K., 2015. Focused ultrasound-mediated drug delivery through the blood–brain barrier. Expert review of neurotherapeutics 15, 477-491.

Chappell, M.A., McConnell, F.A.K., Golay, X., Günther, M., Hernandez-Tamames, J.A., van Osch, M.J. and Asllani, I., 2021. Partial volume correction in arterial spin labeling perfusion MRI: A method to disentangle anatomy from physiology or an analysis step too far?. Neuroimage, *238*, 118236.

Chen, G., Li, H., Shao, X., Wang, D.J., Hu, W., Han, Y., Yang, Q., 2025. Decreased water exchange rate across the blood–brain barrier throughout the Alzheimer's disease continuum: Evidence from Chinese data. Alzheimer's & Dementia 21, e70089.

Chu, P.-C., Liu, H.-L., Lai, H.-Y., Lin, C.-Y., Tsai, H.-C., Pei, Y.-C., 2015. Neuromodulation accompanying focused ultrasound-induced blood-brain barrier opening. Scientific reports 5, 15477.

Cong, X., Kong, W., 2020. Endothelial tight junctions and their regulatory signaling pathways in vascular homeostasis and disease. Cellular signalling 66, 109485.

Daneman, R., Prat, A., 2015. The blood–brain barrier. Cold Spring Harbor perspectives in biology 7, a020412.

Danieli, L., Riccitelli, G., Distefano, D., Prodi, E., Ventura, E., Cianfoni, A., Kaelin-Lang, A., Reinert, M., Pravatà, E., 2019. Brain tumor-enhancement visualization and morphometric assessment: a comparison of MPRAGE, SPACE, and VIBE MRI techniques. American Journal of Neuroradiology 40, 1140-1148.

Deffieux, T. and Konofagou, E.E., 2010. Numerical study of a simple transcranial focused ultrasound system applied to blood-brain barrier opening. IEEE transactions on ultrasonics, ferroelectrics, and frequency control, 57(12), 2637-2653.

Dickie, B.R., Parker, G.J., Parkes, L.M., 2020. Measuring water exchange across the blood-brain barrier using MRI. Progress in Nuclear Magnetic Resonance Spectroscopy 116, 19-39.

Downs, M.E., Teichert, T., Buch, A., Karakatsani, M.E., Sierra, C., Chen, S., Konofagou, E.E., Ferrera, V.P., 2017. Toward a cognitive neural prosthesis using focused ultrasound. Frontiers in Neuroscience 11, 607.

Feshitan, J.A., Chen, C.C., Kwan, J.J. and Borden, M.A., 2009. Microbubble size isolation by differential centrifugation. Journal of colloid and interface science, 329(2), 316-324.

Gulani, V., Calamante, F., Shellock, F.G., Kanal, E., Reeder, S.B., 2017. Gadolinium deposition in the brain: summary of evidence and recommendations. The Lancet Neurology 16, 564-570.

Harvey, H.B., Gowda, V., Cheng, G., 2020. Gadolinium deposition disease: a new risk management threat. Journal of the American College of Radiology 17, 546-550.

Hawkins, B.T., Davis, T.P., 2005. The blood-brain barrier/neurovascular unit in health and disease. Pharmacological reviews 57, 173-185.

Hirt, L., Fukuda, A.M., Ambadipudi, K., Rashid, F., Binder, D., Verkman, A., Ashwal, S., Obenaus, A., Badaut, J., 2017. Improved long-term outcome after transient cerebral ischemia in aquaporin-4 knockout mice. Journal of Cerebral Blood Flow & Metabolism 37, 277-290.

Hynynen, K., McDannold, N., Vykhodtseva, N., Jolesz, F.A., 2001. Noninvasive MR imaging–guided focal opening of the blood-brain barrier in rabbits. Radiology 220, 640-646.

Hývlová, D., Jiřík, R., Vitouš, J., Macíček, O., Krátká, L., Dražanová, E., Starčuk Jr, Z., 2025. Focused ultrasound–induced blood–brain barrier opening: A comparative analysis of permeability quantification based on K trans and PS. Magnetic resonance in medicine 93, 2610-2622.

Jenkinson, M., Beckmann, C.F., Behrens, T.E., Woolrich, M.W., Smith, S.M., 2012. Fsl. Neuroimage 62, 782-790.

Johnson, B.J., Lipford, M.E., Barcus, R.A., Olson, J.D., Schaaf, G.W., Andrews, R.N., Kim, J., Dugan, G.O., Deycmar, S., Reed, C.A. and Whitlow, C.T., 2024. Assessing cerebrovascular reactivity (CVR) in rhesus macaques (Macaca mulatta) using a hypercapnic challenge and pseudo-continuous arterial spin labeling (pCASL). NeuroImage, 285, 120491.

Kanda, T., Ishii, K., Kawaguchi, H., Kitajima, K., Takenaka, D., 2014. High signal intensity in the dentate nucleus and globus pallidus on unenhanced T1-weighted MR images: relationship with increasing cumulative dose of a gadolinium-based contrast material. Radiology 270, 834-841.

Karakatsani, M.E., Pouliopoulos, A.N., Liu, M., Jambawalikar, S.R., Konofagou, E.E., 2020. Contrast-free detection of focused ultrasound-induced blood-brain barrier opening using diffusion tensor imaging. IEEE Transactions on Biomedical Engineering 68, 2499-2508.

Konofagou, E.E., 2012. Optimization of the ultrasound-induced blood-brain barrier opening. Theranostics 2, 1223.

Kovacs, Z.I., Kim, S., Jikaria, N., Qureshi, F., Milo, B., Lewis, B.K., Bresler, M., Burks, S.R., Frank, J.A., 2017. Disrupting the blood–brain barrier by focused ultrasound induces sterile inflammation. Proceedings of the National Academy of Sciences 114, E75-E84.

Kudomi, N., Hayashi, T., Teramoto, N., Watabe, H., Kawachi, N., Ohta, Y., Kim, K.M. and Iida, H., 2005. Rapid quantitative measurement of CMRO2 and CBF by dual administration of 15O-labeled oxygen and water during a single PET scan—a validation study and error analysis in anesthetized monkeys. Journal of Cerebral Blood Flow & Metabolism, 25(9), 1209-1224.

Labriji, W., Clauzel, J., Mestas, J.L., Lafond, M., Lafon, C., Salabert, A.S., Hirschler, L., Warnking, J.M., Barbier, E.L., Loubinoux, I., 2023. Evidence of cerebral hypoperfusion consecutive to ultrasound ‐ mediated blood ‐ brain barrier opening in rats. Magnetic resonance in medicine 89, 2281-2294.

Le Bihan, D., Iima, M., 2015. Diffusion magnetic resonance imaging: what water tells us about biological tissues. PLoS biology 13, e1002203.

Leinenga, G., Langton, C., Nisbet, R., Götz, J., 2016. Ultrasound treatment of neurological diseases—current and emerging applications. Nature Reviews Neurology 12, 161-174.

Li, C.-X., Patel, S., Wang, D.J., Zhang, X., 2014. Effect of high dose isoflurane on cerebral blood flow in macaque monkeys. Magnetic resonance imaging 32, 956-960.

Li, Y., Sadiq, A., Wang, Z., 2022. Arterial spin labelling-based blood-brain barrier assessment and its applications. Investigative magnetic resonance imaging 26, 229.

Li, Y., Ying, Y., Yao, T., Jia, X., Liang, H., Tang, W., Jia, X., Song, H., Shao, X., Wang, D.J., 2023. Decreased water exchange rate across blood–brain barrier in hereditary cerebral small vessel disease. Brain 146, 3079-3087.

Lipsman, N., Meng, Y., Bethune, A.J., Huang, Y., Lam, B., Masellis, M., Herrmann, N., Heyn, C., Aubert, I., Boutet, A., 2018. Blood–brain barrier opening in Alzheimer's disease using MR-guided focused ultrasound. Nature communications 9, 2336.

Liu, D., Munoz, F., Sanatkhani, S., Pouliopoulos, A.N., Konofagou, E.E., Grinband, J., Ferrera, V.P., 2023. Alteration of functional connectivity in the cortex and major brain networks of non-human primates following focused ultrasound exposure in the dorsal striatum. Brain stimulation 16, 1196-1204.

Mahroo, A., Buck, M.A., Huber, J., Breutigam, N.-J., Mutsaerts, H.J., Craig, M., Chappell, M., Günther, M., 2021. Robust multi-TE ASL-based blood–brain barrier integrity measurements. Frontiers in Neuroscience 15, 719676.

Mainprize, T., Lipsman, N., Huang, Y., Meng, Y., Bethune, A., Ironside, S., Heyn, C., Alkins, R., Trudeau, M., Sahgal, A., 2019. Blood-brain barrier opening in primary brain tumors with non-invasive MR-guided focused ultrasound: a clinical safety and feasibility study. Scientific reports 9, 321.

Marquet, F., Teichert, T., Wu, S.-Y., Tung, Y.-S., Downs, M., Wang, S., Chen, C., Ferrera, V., Konofagou, E.E., 2014. Real-time, transcranial monitoring of safe blood-brain barrier opening in non-human primates. PloS one 9, e84310.

McDannold, N., Vykhodtseva, N., Hynynen, K., 2006. Targeted disruption of the blood–brain barrier with focused ultrasound: association with cavitation activity. Physics in Medicine & Biology 51, 793.

McDannold, N., Vykhodtseva, N., Hynynen, K., 2007. Use of ultrasound pulses combined with Definity for targeted blood-brain barrier disruption: a feasibility study. Ultrasound in medicine & biology 33, 584-590.

McMahon, D., Hynynen, K., 2017. Acute inflammatory response following increased blood-brain barrier permeability induced by focused ultrasound is dependent on microbubble dose. Theranostics 7, 3989.

Meng, Y., MacIntosh, B.J., Shirzadi, Z., Kiss, A., Bethune, A., Heyn, C., Mithani, K., Hamani, C., Black, S.E., Hynynen, K., 2019. Resting state functional connectivity changes after MR-guided focused ultrasound mediated blood-brain barrier opening in patients with Alzheimer's disease. Neuroimage 200, 275-280.

Mestre, H., Hablitz, L.M., Xavier, A.L., Feng, W., Zou, W., Pu, T., Monai, H., Murlidharan, G., Castellanos Rivera, R.M., Simon, M.J., 2018. Aquaporin-4-dependent glymphatic solute transport in the rodent brain. Elife 7, e40070.

Ohene, Y., Harrison, I.F., Nahavandi, P., Ismail, O., Bird, E.V., Ottersen, O.P., Nagelhus, E.A., Thomas, D.L., Lythgoe, M.F., Wells, J.A., 2019. Non-invasive MRI of brain clearance pathways using multiple echo time arterial spin labelling: an aquaporin-4 study. Neuroimage 188, 515-523.

Palomares, J.A., Tummala, S., Wang, D.J., Park, B., Woo, M.A., Kang, D.W., Lawrence, K.S.S., Harper, R.M., Kumar, R., 2015. Water exchange across the blood‐brain barrier in obstructive sleep apnea: An MRI diffusion‐weighted pseudo‐continuous arterial spin labeling study. Journal of neuroimaging 25, 900-905.

Papadopoulos, M.C., Verkman, A.S., 2013. Aquaporin water channels in the nervous system. Nature Reviews Neuroscience 14, 265-277.

Pouliopoulos, A.N., Kwon, N., Jensen, G., Meaney, A., Niimi, Y., Burgess, M.T., Ji, R., McLuckie, A.J., Munoz, F.A., Kamimura, H.A. and Teich, A.F., 2021. Safety evaluation of a clinical focused ultrasound system for neuronavigation guided blood-brain barrier opening in non-human primates. Scientific reports, 11(1), 15043.

Pappas, C., Bauer, C.E., Zachariou, V., Maillard, P., Caprihan, A., Shao, X., Wang, D.J., Gold, B.T., 2024. MRI free water mediates the association between water exchange rate across the blood brain barrier and executive function among older adults. Imaging Neuroscience 2, 1-15.

Pouliopoulos, A.N., Kwon, N., Jensen, G., Meaney, A., Niimi, Y., Burgess, M.T., Ji, R., McLuckie, A.J., Munoz, F.A., Kamimura, H.A., 2021. Safety evaluation of a clinical focused ultrasound system for neuronavigation guided blood-brain barrier opening in non-human primates. Scientific reports 11, 15043.

Rezai, A.R., Ranjan, M., D'Haese, P.-F., Haut, M.W., Carpenter, J., Najib, U., Mehta, R.I., Chazen, J.L., Zibly, Z., Yates, J.R., 2020. Noninvasive hippocampal blood− brain barrier opening in Alzheimer's disease with focused ultrasound. Proceedings of the National Academy of Sciences 117, 9180-9182.

Rigollet, S., Rome, C., Ador, T., Dumont, E., Pichon, C., Delalande, A., Barbier, E.L., Stupar, V., 2024. FUS-mediated BBB opening leads to transient perfusion decrease and inflammation without acute or chronic brain lesion. Theranostics 14, 4147.

Shao, X., Jann, K., Ma, S.J., Yan, L., Montagne, A., Ringman, J.M., Zlokovic, B.V., Wang, D.J., 2020. Comparison between blood-brain barrier water exchange rate and permeability to gadolinium-based contrast agent in an elderly cohort. Frontiers in Neuroscience 14, 571480.

Shao, X., Ma, S.J., Casey, M., D' Orazio, L., Ringman, J.M., Wang, D.J., 2019. Mapping water exchange across the blood‐brain barrier using 3D diffusion‐prepared arterial spin labeled perfusion MRI. Magnetic resonance in medicine 81, 3065-3079.

Shao, X., Shou, Q., Felix, K., Ojogho, B., Jiang, X., Gold, B.T., Herting, M.M., Goldwaser, E.L., Kochunov, P., Hong, E., 2024. Age-related decline in blood-brain barrier function is more pronounced in males than females in parietal and temporal regions. Elife 13, RP96155.

Shao, X., Zhao, C., Shou, Q., St Lawrence, K.S., Wang, D.J., 2023. Quantification of blood‐brain barrier water exchange and permeability with multidelay diffusion‐weighted pseudo‐continuous arterial spin labeling. Magnetic resonance in medicine 89, 1990-2004.

Sheikov, N., McDannold, N., Vykhodtseva, N., Jolesz, F., Hynynen, K., 2004. Cellular mechanisms of the blood-brain barrier opening induced by ultrasound in presence of microbubbles. Ultrasound in medicine & biology 30, 979-989.

Slupe, A.M. and Kirsch, J.R., 2018. Effects of anesthesia on cerebral blood flow, metabolism, and neuroprotection. Journal of Cerebral Blood Flow & Metabolism, 38(12), 2192-2208.

Sourbron, S.P., Buckley, D.L., 2013. Classic models for dynamic contrast‐enhanced MRI. NMR in Biomedicine 26, 1004-1027.

St. Lawrence, K.S., Owen, D., Wang, D.J., 2012. A two‐stage approach for measuring vascular water exchange and arterial transit time by diffusion‐weighted perfusion MRI. Magnetic resonance in medicine 67, 1275-1284.

Sun, T., Samiotaki, G., Wang, S., Acosta, C., Chen, C.C., Konofagou, E.E., 2015. Acoustic cavitation-based monitoring of the reversibility and permeability of ultrasound-induced blood-brain barrier opening. Physics in Medicine & Biology 60, 9079.

Sweeney, M.D., Zhao, Z., Montagne, A., Nelson, A.R., Zlokovic, B.V., 2018. Blood-brain barrier: from physiology to disease and back. Physiological reviews.

Tang, G., Liu, Y., Zhang, Z., Lu, Y., Wang, Y., Huang, J., Li, Y., Chen, X., Gu, X., Wang, Y., 2014. Mesenchymal stem cells maintain blood-brain barrier integrity by inhibiting aquaporin-4 upregulation after cerebral ischemia. Stem Cells 32, 3150-3162.

Tiwari, Y.V., Lu, J., Shen, Q., Cerqueira, B. and Duong, T.Q., 2017. Magnetic resonance imaging of blood–brain barrier permeability in ischemic stroke using diffusion-weighted arterial spin labeling in rats. Journal of Cerebral Blood Flow & Metabolism, *37*(8), 2706-2715.

Tiwari, Y.V., Muir, E.R., Jiang, Z., Duong, T.Q., 2025. Diffusion-weighted arterial spin labeling MRI to investigate mannitol-induced blood brain barrier disruption. Magnetic resonance imaging, 110335.

Todd, N., Zhang, Y., Arcaro, M., Becerra, L., Borsook, D., Livingstone, M., McDannold, N., 2018. Focused ultrasound induced opening of the blood-brain barrier disrupts inter-hemispheric resting state functional connectivity in the rat brain. Neuroimage 178, 414-422.

Todd, N., Zhang, Y., Livingstone, M., Borsook, D., McDannold, N., 2019. The neurovascular response is attenuated by focused ultrasound-mediated disruption of the blood-brain barrier. Neuroimage 201, 116010.

Tung, Y.-S., Marquet, F., Teichert, T., Ferrera, V., Konofagou, E.E., 2011. Feasibility of noninvasive cavitation-guided blood-brain barrier opening using focused ultrasound and microbubbles in nonhuman primates. Applied physics letters 98.

Uchida, Y., Kan, H., Sakurai, K., Oishi, K., Matsukawa, N., 2023. Contributions of blood–brain barrier imaging to neurovascular unit pathophysiology of Alzheimer's disease and related dementias. Frontiers in Aging Neuroscience 15, 1111448.

Vlachos, F., Tung, Y., Konofagou, E., 2010. Permeability assessment of the focused ultrasound-induced blood–brain barrier opening using dynamic contrast-enhanced MRI. Physics in Medicine & Biology 55, 5451.

Wang, J., Alsop, D.C., Song, H.K., Maldjian, J.A., Tang, K., Salvucci, A.E., Detre, J.A., 2003. Arterial transit time imaging with flow encoding arterial spin tagging (FEAST). Magnetic Resonance in Medicine: An Official Journal of the International Society for Magnetic Resonance in Medicine 50, 599-607.

Wang, J., Fernández-Seara, M.A., Wang, S., Lawrence, K.S.S., 2007. When perfusion meets diffusion: in vivo measurement of water permeability in human brain. Journal of Cerebral Blood Flow & Metabolism 27, 839-849.

Wengler, K., Ha, J., Syritsyna, O., Bangiyev, L., Coyle, P.K., Duong, T.Q., Schweitzer, M.E., He, X., 2020. Abnormal blood-brain barrier water exchange in chronic multiple sclerosis lesions: A preliminary study. Magnetic resonance imaging 70, 126-133.

Wu, S.Y., Aurup, C., Sanchez, C.S., Grondin, J., Zheng, W., Kamimura, H., Ferrera, V.P. and Konofagou, E.E., 2018. Efficient blood-brain barrier opening in primates with neuronavigation-guided ultrasound and real-time acoustic mapping. Scientific reports, 8(1), 7978.

Xu, X., Chan, K.W., Knutsson, L., Artemov, D., Xu, J., Liu, G., Kato, Y., Lal, B., Laterra, J., McMahon, M.T., 2015. Dynamic glucose enhanced (DGE) MRI for combined imaging of blood–brain barrier break down and increased blood volume in brain cancer. Magnetic resonance in medicine 74, 1556-1563.

Zhang, X., Nagaoka, T., Auerbach, E.J., Champion, R., Zhou, L., Hu, X. and Duong, T.Q., 2007. Quantitative basal CBF and CBF fMRI of rhesus monkeys using three-coil continuous arterial spin labeling. Neuroimage, 34(3), pp.1074-1083.

Zhang, X., 2022. Effects of anesthesia on cerebral blood flow and functional connectivity of nonhuman primates. *Veterinary Sciences*, *9*(10), p.516.

Zeppenfeld, D.M., Simon, M., Haswell, J.D., D'Abreo, D., Murchison, C., Quinn, J.F., Grafe, M.R., Woltjer, R.L., Kaye, J., Iliff, J.J., 2017. Association of perivascular localization of aquaporin-4 with cognition and Alzheimer disease in aging brains. JAMA neurology 74, 91-99.